

## Article

# Probing Electron Excitation Characters of Carboline-Based Bis-Tridentate Ir(III) Complexes

 Jie Yan <sup>1,†</sup>, Ze-Lin Zhu <sup>2,†</sup>, Chun-Sing Lee <sup>2,\*</sup>, Shih-Hung Liu <sup>3</sup>, Pi-Tai Chou <sup>3,\*</sup> and Yun Chi <sup>1,2,\*</sup> 

- <sup>1</sup> Department of Materials Science and Engineering, City University of Hong Kong, Hong Kong SAR, China; jyanae@connect.ust.hk
- <sup>2</sup> Center of Super-Diamond and Advanced Films (COSDAF) and Department of Chemistry, City University of Hong Kong, Hong Kong SAR, China; zelinzhu-c@my.cityu.edu.hk
- <sup>3</sup> Department of Chemistry, National Taiwan University, Taipei 10617, Taiwan; d96223131@ntu.edu.tw
- \* Correspondence: apcslee@cityu.edu.hk (C.-S.L.); chop@ntu.edu.tw (P.-T.C.); yunchi@cityu.edu.hk (Y.C.)
- † These authors contributed equally to this work.

**Abstract:** In this work, we report a series of bis-tridentate Ir(III) metal complexes, comprising a dianionic pyrazole-pyridine-phenyl tridentate chelate and a monoanionic chelate bearing a peripheral carbene and carboline coordination fragment that is linked to the central phenyl group. All these Ir(III) complexes were synthesized with an efficient one-pot and two-step method, and their emission hue was fine-tuned by variation of the substituent at the central coordination entity (i.e., pyridinyl and phenyl group) of each of the tridentate chelates. Their photophysical and electrochemical properties, thermal stabilities and electroluminescence performances are examined and discussed comprehensively. The doped devices based on [Ir(cbF)(phyz1)] (**Cb1**) and [Ir(cbB)(phyz1)] (**Cb4**) give a maximum external quantum efficiency (current efficiency) of 16.6% (55.2 cd/A) and 13.9% (43.8 cd/A), respectively. The relatively high electroluminescence efficiencies indicate that bis-tridentate Ir(III) complexes are promising candidates for OLED applications.

**Keywords:** bis-tridentate Ir(III) complex; carboline; carbene OLED; substituent effect



**Citation:** Yan, J.; Zhu, Z.-L.; Lee, C.-S.; Liu, S.-H.; Chou, P.-T.; Chi, Y. Probing Electron Excitation Characters of Carboline-Based Bis-Tridentate Ir(III) Complexes. *Molecules* **2021**, *26*, 6048. <https://doi.org/10.3390/molecules26196048>

Academic Editor: Takashi Akitsu

Received: 13 September 2021

Accepted: 30 September 2021

Published: 6 October 2021

**Publisher's Note:** MDPI stays neutral with regard to jurisdictional claims in published maps and institutional affiliations.



**Copyright:** © 2021 by the authors. Licensee MDPI, Basel, Switzerland. This article is an open access article distributed under the terms and conditions of the Creative Commons Attribution (CC BY) license (<https://creativecommons.org/licenses/by/4.0/>).

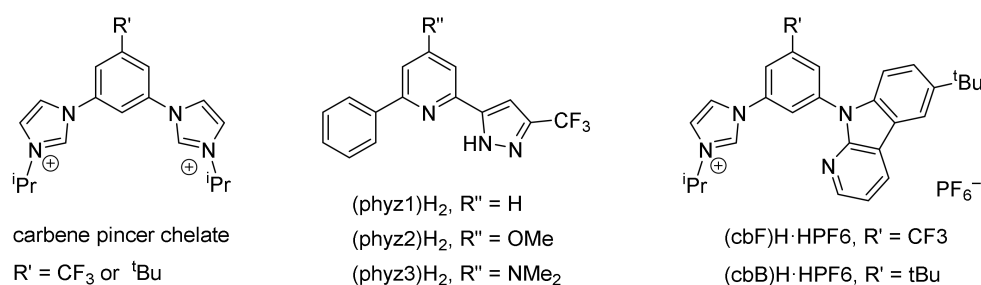
## 1. Introduction

Organic light-emitting diodes (OLEDs) have been widely employed in the fabrication of flat panel displays and solid-state lighting luminaries. In this regard, Ir(III) phosphors have received special attention for their capability in harvesting both the singlet and triplet excited states formed in the devices [1]. The triplet states account for 75% of the total excited states generated; hence, the strong spin-orbit coupling exerted by the Ir(III) metal atom can reduce the radiative lifetime of triplet excited states, resulting in a significant improvement of the overall efficiency of OLEDs. This has triggered numerous studies on the quest of chemically and photochemically stable Ir(III) metal complexes, to which the efficient phosphorescence from the coupled ligand-centered (LC)  $\pi\pi^*$  and metal-to-ligand charge transfer (MLCT) excited states tend to fulfil the criteria for higher OLED efficiency [2–7].

Traditionally, these Ir(III) emitters were constructed using bidentate cyclometalates such as 2-phenylpyridine or functional analogues (C^N) and/or monoanionic ancillary chelate, denoted as (L^X). The tris-homoleptic and heteroleptic Ir(III) complexes [Ir(C^N)<sub>3</sub>] and [Ir(C^N)<sub>2</sub>(L^X)] have been extensively designed and studied [8]. In theory, both of them are capable of affording at least two stereoisomers, which are controlled by their intrinsic kinetic and thermodynamic factors. They are named as *fac*- (facial) and *mer*- (meridional) isomers in the case of homoleptic complexes [Ir(C^N)<sub>3</sub>]. Generally, these stereoisomers possess distinctive chemical and physical properties and, hence, their interconversion should be limited during preparation. One possible method in preventing the formation of multiple stereoisomers is to employ the bis-tridentate architectures, to which the planar

motif of tridentate chelates are well-known for preventing formation of conformational isomers in the octahedral coordination framework [9–11].

Studies on charge-neutral bis-tridentate Ir(III) complexes are limited [12,13], despite a hefty compilation of studies on analogous ionic complexes [14–16]. For the former, Williams and co-workers obtained these Ir(III) complexes by controlled blockage of the reactive site on the chelate [17]. Koga reported the bis-tridentate Ir(III) complex with both pyridylbiphenyl and phenylbipyridyl cyclometalate [18]. Furthermore, bis-tridentate architecture was also extended to carbazoly-, phenoxy- and benzimidazol-2-yl-based chelates with an improved photoluminescence yield, as reported by Esteruelas et al. [19,20]. In the meantime, Chi and co-workers sought to explore efficient RGB emitters with pincer carbene ancillary (Scheme 1), aimed for potential OLED applications [21–24]. Later on, the 2-phenyl-6-(3-(trifluoromethyl)-1H-pyrazol-5-yl)pyridine system (phyzn) $H_2$  ( $n = 1, 2$  and  $3$ ), which could serve as both the monoanionic and dianionic chelate depending on the synthetic manipulation for preparation of emissive Ir(III) complexes, attracted research attention [25–28]. Given this background, we decided to use these aforementioned (phyzn) $H_2$  chelates, together with carbene-benzene-carboline pro-chelates (cbF)H·HF $_6$  and (cbB)H·HF $_6$ , in building the bis-tridentate Ir(III) complexes. A carboline fragment was selected as the key component of this monoionic chelate, as it has been involved in preparation of bi-dentate chelates for Ir(III) metal complexes [29,30] that have exceptional electronic properties in various bipolar host materials [31–35]. Finally, within these tridentate chelates, the carboline N-donor will reside *trans*- to the peripheral carbene unit, avoiding the putative *trans*-influence that may exist in the coordinated carbene pincer chelates.



**Scheme 1.** Structural drawings of both the carbene pincer chelate and chelates employed in the present study.

## 2. Experimental Section

### 2.1. General Information

All solvents were dried and degassed before used, and commercially available reagents were used without further purification. 2,6-Dibromo-4-methoxypyridine [36,37], 2,6-dibromo-*N,N*-dimethylpyridin-4-amine [38,39] and 6-(*tert*-butyl)-9H-pyrido[2,3-*b*]indole [40] were prepared using methods reported in literature. All reactions were conducted under N $_2$  atmosphere and monitored by precoated TLC plates (0.20 nm with fluorescent indicator F254).  $^1$ H and  $^{19}$ F spectra were recorded with Bruker 400 MHz AVANCE III Nuclear Magnetic Resonance System. Elemental analysis was performed by an elemental carbon-hydrogen-nitrogen analyzer (Elementar). Mass spectra were obtained on 4800 Plus MALDI TOF/TOF Analyzer (ABI), where 2,5-dihydroxybenzoic acid was applied as the matrix. TGA measurements were performed on a TA Instrument TGAQ50, at a heating rate of 10 °C min $^{-1}$  under N $_2$  atmosphere. The X-ray intensity data were measured using phi and omega scan modes (APEX3) at 233 K on a Bruker D8 Venture Photon II diffractometer with microfocus X-ray sources.

### 2.2. Synthesis of the Bis-Tridentate Ir(III) Metal Complexes Cb1–5

**Synthesis of [Ir(cbF)(phyz1)] (Cb1):** A mixture of (cbF)H·HF $_6$  (186 mg, 0.3 mmol), [Ir(COD)Cl] $_2$  (100 mg, 0.15 mmol) and NaOAc (123 mg, 1.5 mmol) in 15 mL of degassed acetonitrile was refluxed for 12 h. After, the solvent was removed and the resulting residue

was added of (phyz1)H<sub>2</sub> (86.4 mg, 0.3 mmol), 10 mL of decalin and NaOAc (123 mg, 1.5 mmol). This mixture was refluxed for another 24 h and, after removal of decalin under reduced pressure, the residue was taken into CH<sub>2</sub>Cl<sub>2</sub> (30 mL × 3) and the combined solution was washed with deionized water. Finally, the organic layer was dried over Na<sub>2</sub>SO<sub>4</sub>, and filtered and concentrated to dryness. The residue was purified by column chromatography (SiO<sub>2</sub>, ethyl acetate/hexane = 1:3) to yield 180 mg of yellow solid, 0.19 mmol, which is calculated to be a yield of 62%.

Other bis-tridentate Ir(III) derivatives, i.e., [Ir(cbF)(phyz2)] (**Cb2**), [Ir(cbF)(phyz3)] (**Cb3**), [Ir(cbB)(phyz1)] (**Cb4**) and [Ir(cbB)(phyz3)] (**Cb5**), were synthesized from condensation of the carboline-based chelates (cbF)H·HF<sub>6</sub> and (cbB)H·HF<sub>6</sub> with respective dianionic chelates (phyz1)H<sub>2</sub>, (phyz2)H<sub>2</sub> and (phyz3)H<sub>2</sub> under similar reaction conditions.

Spectral data of **Cb1**: MS (MALDI-TOF, <sup>193</sup>Ir): *m/z* 956.27637 [M + H<sup>+</sup>]; <sup>1</sup>H NMR (400 MHz, acetone-d<sub>6</sub>, 296 K) δ = 8.55 (dd, *J* = 7.6, 1.2 Hz, 1H), 8.35 (d, *J* = 9.2 Hz, 1H), 8.32 (d, *J* = 2.0 Hz, 1H), 8.12–8.15 (m, 3H), 8.04 (d, *J* = 8.0 Hz, 1H), 7.97 (d, *J* = 8.0 Hz, 1H), 7.87 (dd, *J* = 8.8, 2.0 Hz, 1H), 7.83 (s, 1H), 7.75 (d, *J* = 8.0 Hz, 1H), 7.42 (dd, *J* = 5.6, 1.2 Hz, 1H), 7.20 (d, *J* = 2.0 Hz, 1H), 7.06 (s, 1H), 6.98 (dd, *J* = 7.2, 5.6 Hz, 1H), 6.76–6.82 (m, 1H), 6.60 (td, *J* = 7.2, 1.2 Hz, 1H), 6.50–6.46 (m, 1H), 3.43–3.49 (m, 1H), 1.46 (s, 9H), 0.88 (d, *J* = 6.8 Hz, 6H); <sup>19</sup>F NMR (376 MHz, acetone-d<sub>6</sub>, 296 K): δ = −60.39 (s, 3F), −61.46 (s, 3F). Analytical data: calculated for C<sub>43</sub>H<sub>34</sub>F<sub>6</sub>IrN<sub>7</sub>: C, 54.08; H, 3.59; F, 11.94; Ir, 20.13; N, 10.27. Found: C, 54.10; H, 3.57; N, 10.56.

Spectral data of **Cb2**: a yellow solid, with a yield of 51%. MS (MALDI-TOF, <sup>193</sup>Ir): *m/z* 986.32111 [M + H<sup>+</sup>]; <sup>1</sup>H NMR (400 MHz, acetone-d<sub>6</sub>, 296 K) δ = 8.54 (d, *J* = 6.4 Hz, 1H), 8.34 (d, *J* = 8.8 Hz, 1H), 8.31 (d, *J* = 2.0 Hz, 1H), 8.13 (d, *J* = 2.0 Hz, 1H), 8.11 (s, 1H), 7.86 (dd, *J* = 8.8, 2.0 Hz, 1H), 7.82 (s, 1H), 7.75 (d, *J* = 7.6 Hz, 1H), 7.65 (s, 2H), 7.47 (d, *J* = 5.2 Hz, 1H), 7.19 (d, *J* = 2.0 Hz, 1H), 7.08 (s, 1H), 7.00 (dd, *J* = 7.2, 6.0 Hz, 1H), 6.77 (t, *J* = 7.6 Hz, 1H), 6.58 (t, *J* = 7.2 Hz, 1H), 6.45 (d, *J* = 7.6 Hz, 1H), 4.24 (s, 3H), 3.56–3.62 (m, 1H), 1.46 (s, 9H), 0.91 (dd, *J* = 6.8, 4.4 Hz, 6H); <sup>19</sup>F NMR (376 MHz, acetone-d<sub>6</sub>, 296 K): δ = −60.36 (s, 3F), −61.40 (s, 3F). Analytical data: calculated for C<sub>44</sub>H<sub>36</sub>F<sub>6</sub>IrN<sub>7</sub>O: C, 53.65; H, 3.68; F, 11.57; Ir, 19.51; N, 9.95; O, 1.62. Found: C, 53.81; H, 3.78; N, 9.85.

Spectral data of **Cb3**: a yellow solid with a yield of 50%. MS (MALDI-TOF, <sup>193</sup>Ir): *m/z* 999.31921 [M + H<sup>+</sup>]; <sup>1</sup>H NMR (400 MHz, acetone-d<sub>6</sub>, 296 K) δ = 8.54 (d, *J* = 7.2 Hz, 1H), 8.33 (d, *J* = 8.8 Hz, 1H), 8.31 (s, 1H), 8.08–8.13 (m, 2H), 7.85 (d, *J* = 8.8, 2.0 Hz, 1H), 7.79 (s, 1H), 7.72 (d, *J* = 7.6 Hz, 1H), 7.55 (d, *J* = 5.6 Hz, 1H), 7.37 (d, *J* = 9.6 Hz, 2H), 7.19 (d, *J* = 2.4 Hz, 1H), 6.96–7.03 (m, 2H), 6.72 (t, *J* = 7.2 Hz, 1H), 6.52 (t, *J* = 7.2 Hz, 1H), 6.40 (d, *J* = 7.2 Hz, 1H), 3.69–3.76 (m, 1H), 3.43 (s, 6H), 1.46 (s, 9H), 0.89–0.93 (m, 6H); <sup>19</sup>F NMR (376 MHz, acetone-d<sub>6</sub>, 296 K): δ = −60.20 (s, 3F), −61.35 (s, 3F). Analytical data: calculated for C<sub>45</sub>H<sub>39</sub>F<sub>6</sub>IrN<sub>8</sub>: C, 54.15; H, 3.94; F, 11.42; Ir, 19.26; N, 11.23. Found: C, 54.43; H, 3.85; N, 10.98.

Spectral data of **Cb4**: a yellow solid with a yield of 54%. MS (MALDI-TOF, <sup>193</sup>Ir): *m/z* 944.34766 [M + H<sup>+</sup>]; <sup>1</sup>H NMR (400 MHz, acetone-d<sub>6</sub>, 296 K): δ = 8.50 (d, *J* = 7.6 Hz, 1H), 8.43 (d, *J* = 9.2 Hz, 1H), 8.29 (d, *J* = 2.0 Hz, 1H), 8.08 (t, *J* = 8.0 Hz, 1H), 8.02 (d, *J* = 2.0 Hz, 1H), 7.97–8.02 (m, 2H), 7.94 (d, *J* = 7.6 Hz, 1H), 7.84 (dd, *J* = 8.8, 2.0 Hz, 1H), 7.71 (d, *J* = 7.6 Hz, 1H), 7.61 (s, 1H), 7.41 (d, *J* = 5.6 Hz, 1H), 7.10 (d, *J* = 2.4 Hz, 1H), 7.04 (s, 1H), 6.91 (dd, *J* = 7.6, 6.0 Hz, 1H), 6.72–6.77 (m, 1H), 6.50–6.58 (m, 2H), 3.41–3.48 (m, 1H), 1.58 (s, 9H), 1.46 (s, 9H), 0.85 (d, *J* = 6.8 Hz, 6H); <sup>19</sup>F NMR (376 MHz, acetone-d<sub>6</sub>, 296 K): δ = −60.26 (s, 3F). Analytical data: calculated for C<sub>46</sub>H<sub>43</sub>F<sub>3</sub>IrN<sub>7</sub>: C, 58.58; H, 4.60; F, 6.04; Ir, 20.38; N, 10.40. Found: C, 58.50; H, 4.53; N, 10.54.

Spectral data of **Cb5**: a greenish solid with a yield of 52%. MS (MALDI-TOF, <sup>193</sup>Ir): *m/z* 987.43604 [M + H<sup>+</sup>]; <sup>1</sup>H NMR (400 MHz, acetone-d<sub>6</sub>, 296 K): δ = 8.49 (d, *J* = 7.2 Hz, 1H), 8.42 (d, *J* = 8.8 Hz, 1H), 8.28 (d, *J* = 2.0 Hz, 1H), 7.99 (d, *J* = 2.0 Hz, 1H), 7.95 (s, 1H), 7.82 (dd, *J* = 8.8, 2.0 Hz, 1H), 7.67 (d, *J* = 8.0 Hz, 1H), 7.57 (s, 1H), 7.54 (d, *J* = 6.0 Hz, 1H), 7.36 (d, *J* = 2.0 Hz, 1H), 7.32 (s, 1H), 7.08 (d, *J* = 2.0 Hz, 1H), 6.98 (s, 1H), 6.92 (dd, *J* = 7.6, 6.0 Hz, 1H), 6.64–6.71 (m, 1H), 6.46–6.47 (m, 2H), 3.67–3.73 (m, 1H), 3.41 (s, 6H), 1.57 (s, 9H), 1.46 (s, 9H), 0.88 (m, 6H); <sup>19</sup>F NMR (376 MHz, acetone-d<sub>6</sub>, 296 K): δ = −60.08 (s, 6F). Analytical

data: calculated for  $C_{48}H_{48}F_3IrN_8$ : C, 58.46; H, 4.91; F, 5.78; Ir, 19.49; N, 11.36. Found: C, 58.37; H, 4.93; N, 11.14.

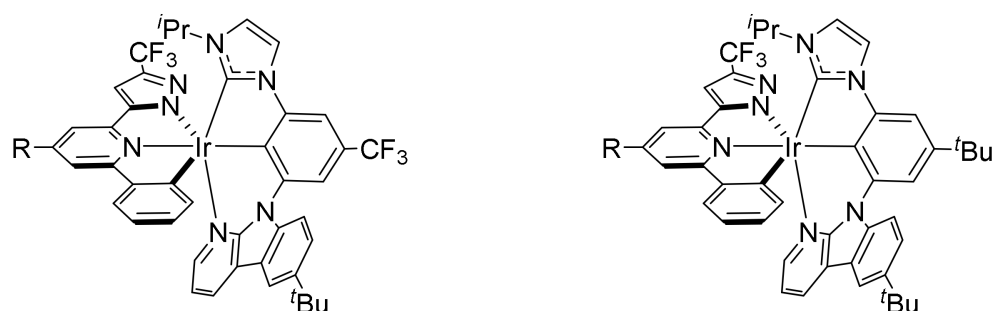
Selected crystal data of **Cb1**: CCDC deposition number: 2095978.  $C_{43}H_{36}F_6IrN_7O$ ;  $M = 972.99$ ; orthorhombic; space group = *Pbca* (No. 61);  $a = 22.6543(5)$  Å,  $b = 15.0837(3)$  Å,  $c = 27.9723(6)$  Å;  $V = 9558.4(4)$  Å<sup>3</sup>;  $Z = 8$ ;  $\rho_{\text{Calcd}} = 1.352$  g·cm<sup>-3</sup>;  $F(000) = 3856$ , crystal size =  $0.49 \times 0.05 \times 0.04$  mm<sup>3</sup>;  $\lambda(\text{CuK}\alpha) = 1.54178$  Å;  $T = 213(2)$  K;  $\mu = 5.925$  mm<sup>-1</sup>; 83,799 reflections collected, 9741 independent reflections ( $R_{\text{int}} = 0.0740$ ,  $R_{\sigma} = 0.0444$ ); max. and min. transmission = 0.365 and 0.754, respectively; data/restraints/parameters = 9741/354/621; GOF = 1.041; final  $R_1[I > 2\sigma(I)] = 0.0296$  and  $wR_2(\text{all data}) = 0.0764$ . All deposited data can be obtained free of charge on application to CCDC, 12 Union Road, Cambridge CB21EZ, UK (fax: (+44) 1223-336-033; e-mail: deposit@ccdc.cam.ac.uk).

### 3. Results and Discussion

#### 3.1. Syntheses and Characterizations

Synthesis of dianionic chelate  $(\text{phyzn})\text{H}_2$  ( $n = 1, 2$  and  $3$ ) followed the literature precedents [37,41]. Commercially available 2,6-dibromopyridine and self-synthesized 2,6-dibromo-4-methoxypyridine [36] and 2,6-dibromo-*N,N*-dimethylpyridin-4-amine [38,39] were employed as the respective starting materials. For preparation of the carbene-benzene-carboline pro-chelates  $(\text{cbF})\text{H}\cdot\text{HF}_6$  and  $(\text{cbB})\text{H}\cdot\text{HF}_6$ , 1,3-dibromo-5-(trifluoromethyl)benzene and 1,3-dibromo-5-(*tert*-butyl)benzene were first coupled with functional  $\alpha$ -carboline using the multi-step protocol described in Scheme S2 of electronic supporting information (ESI). The isolated intermediates were next reacted with imidazole in presence of both CuO and  $\text{K}_2\text{CO}_3$ , followed by methylation of peripheral imidazole in giving the *N*-methyl imidazolium entity. Finally, their iodide anion was metathesized with  $\text{PF}_6^-$  anion with addition of excessive, aqueous  $\text{KPF}_6$ , giving an immediate precipitation of a white solid of  $(\text{cbF})\text{H}\cdot\text{HF}_6$  and  $(\text{cbB})\text{H}\cdot\text{HF}_6$  as the intended tridentate chelates.

After that, the preparation of the bis-tridentate Ir(III) complexes **Cb1–5** was conducted using a one-pot and two-step method. As a generalized protocol, the carboline chelate  $(\text{cbF})\text{H}\cdot\text{HF}_6$  (or  $(\text{cbB})\text{H}\cdot\text{HF}_6$ ) was first heated with  $[\text{Ir}(\text{COD})\text{Cl}]_2$  and sodium acetate in degassed acetonitrile. The intermediate was next reacted with a series of second chelate  $(\text{phyzn})\text{H}_2$  ( $n = 1, 2$  and  $3$ ) in decalin to afford the desired Ir(III) complexes in moderate yields. The mass spectrometry and <sup>1</sup>H and <sup>19</sup>F NMR spectroscopies, together with a single crystal X-ray diffraction study on **Cb1**, were examined to offer the needed characterizations. Their structural drawings are depicted in Scheme 2 for scrutiny.



**Cb1**, R = H; **Cb2**, R = OMe; **Cb3**, R = NMe<sub>2</sub>      **Cb4**, R = H; **Cb5**, R = NMe<sub>2</sub>

**Scheme 2.** Structural drawings of the bis-tridentate Ir(III) complexes **Cb1–5**.

Figure 1 depicts the molecular drawing of **Cb1**, with thermal ellipsoids drawn at a level of 30% probability. The crystal of **Cb1** for X-ray diffraction was obtained via the slow diffusion of hexane into a saturated  $\text{CH}_2\text{Cl}_2$  solution of **Cb1** at RT. The Ir(III) metal atom constituted a slightly distorted octahedral coordination arrangement with two mutually orthogonal tridentate chelates. The *phyz1* chelate is essentially planar, while that of the tridentate chelate *cbF* underwent a slight distortion at the outer hexagonal

ring of the carboline unit, which can be attributed to the unfavourable steric interaction between carboline and central benzene fragments. In agreement with the prediction of trans-influence [42], the carbene Ir-C distance (Ir-C(39) = 2.004(3) Å) is relatively shorter than the typical Ir-C distances observed in other bis-tridentate Ir(III) complexes bearing symmetrically arranged carbene pincer chelates (2.043 – 2.062 Å) [43,44]. Concomitantly, the Ir-C distance of central benzene group (Ir-C(31) = 2.011(3) Å) elongated slightly in comparison to that of the corresponding carbene pincer chelates (1.950–1.960 Å).

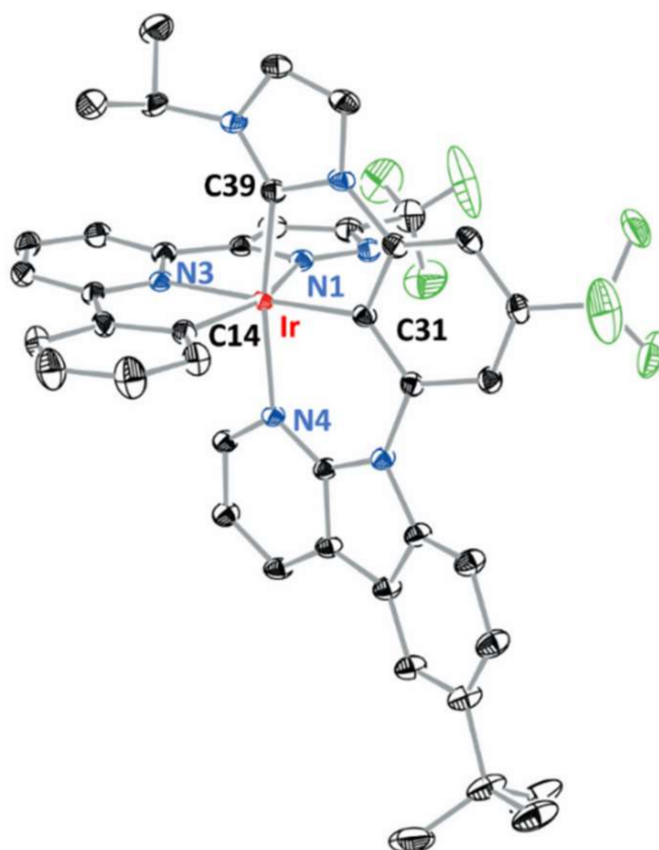


**Figure 1.** Structural drawing of **Cb1** with ellipsoids shown at 30% probability. Nitrogen atoms in blue, carbon atoms in black, iridium atom in red, fluorine atoms in green. All hydrogen atoms are omitted for clarity. Selected bond distances: Ir-N(1) = 2.149(3), Ir-N(3) = 2.055(3), Ir-N(4) = 2.120(3), Ir-C(14) = 2.019(4), Ir-C(31) = 2.011(3) and Ir-C(39) = 2.004(3) Å; Selected bond angles: C(14)-Ir-N(1) = 156.82(14), C(39)-Ir-N(4) = 169.77(14), C(31)-Ir-N(4) = 89.79(13) and C(31)-Ir-N(3) = 177.19(13)°.

### 3.2. Photophysical and Electrochemical Properties

Figure 2 reveals both the absorption and emission spectra of **Cb1–5** recorded in the degassed  $\text{CH}_2\text{Cl}_2$  solution, to which the corresponding photophysical data are summarized in Table 1. All Ir(III) complexes give similar absorption patterns, and the higher energy bands above 380 nm are attributed to the spin-allowed  $\pi\pi^*$  transition, while those occurring at the longer wavelength regions of 380–450 nm are assigned to the singlet metal-to-ligand charge transfer ( $^1\text{MLCT}$ ). The next lower absorption bands spanning the region from 450 nm up to the onset are ascribed to the mixed spin-forbidden ligand-centered  $\pi\pi^*$  transition and MLCT transition processes.

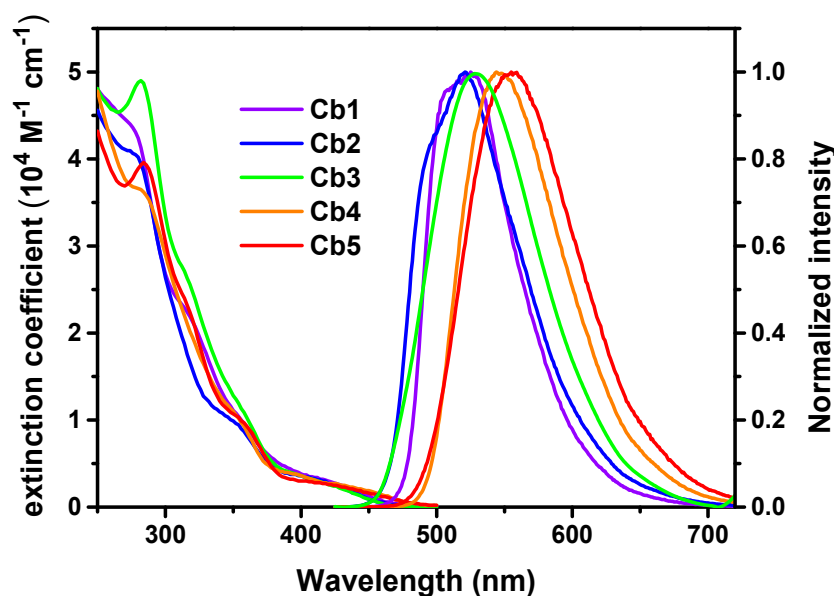


Figure 2. UV–vis absorption and normalized emission spectra of the studied Ir(III) complexes Cb1–5 in degassed CH<sub>2</sub>Cl<sub>2</sub> solution at RT.

Table 1. The corresponding photophysical properties of Ir(III) complexes Cb1–5 in degassed CH<sub>2</sub>Cl<sub>2</sub> solution at RT.

	$\lambda_{\text{abs}}$ (nm); ( $\epsilon \times 10^4 \text{ M}^{-1} \text{ cm}^{-1}$ ) <sup>[a]</sup>	$\lambda_{\text{em}}$ (nm) <sup>[b]</sup>	$\Phi$ (%) <sup>[b,c]</sup>	$\tau_{\text{obs}}$ ( $\mu\text{s}$ ) <sup>[b]</sup>	$k_r$ ( $\text{s}^{-1}$ ) <sup>[d]</sup>	$k_{\text{nr}}$ ( $\text{s}^{-1}$ ) <sup>[d]</sup>
Cb1	278 (4.31), 318 (2.19), 358 (0.96), 420 (0.3)	506(sh), 525	69	3.4	$2.0 \times 10^5$	$0.91 \times 10^5$
Cb2	280 (4.02), 352 (0.96), 416 (0.3)	495(sh), 521	48	1.5	$3.2 \times 10^5$	$3.4 \times 10^5$
Cb3	282 (4.9), 316 (2.63), 358 (1.09), 418 (0.28)	529	41	1.2	$3.4 \times 10^5$	$4.9 \times 10^5$
Cb4	284 (3.62), 354 (1.02), 398 (0.37), 446 (0.2)	544	58	2.0	$2.9 \times 10^5$	$2.1 \times 10^5$
Cb5	284 (3.96), 316 (2.32), 356(0.99), 418 (0.27)	555	46	1.4	$3.3 \times 10^5$	$3.8 \times 10^5$

<sup>[a]</sup> UV-vis spectra were recorded in CH<sub>2</sub>Cl<sub>2</sub> at a concentration  $10^{-5}$  M at RT; <sup>[b]</sup> PL spectra, lifetime, and quantum yields were recorded in degassed CH<sub>2</sub>Cl<sub>2</sub> at RT; <sup>[c]</sup> Coumarin (C153) in EtOH (Q.Y. = 58% and  $\lambda_{\text{max}}$  = 530 nm) was employed as standard; <sup>[d]</sup>  $k_r$  = radiative decay rate constant and  $k_{\text{nr}}$  = nonradiative decay rate constant.

Upon photoexcitation, an intense green emission was observed among Cb1, Cb2 and Cb3 in the degassed CH<sub>2</sub>Cl<sub>2</sub> solution with the peak wavelength at 525, 521 and 529 nm, respectively. The slight shifting of peak indicates the substituent effects of the pyridinyl coordination unit. It is worth noting that the shoulder at the right of emission profile gradually vanished in accordance with the sequence of hydrogen, methoxy, dimethylamino presented, manifesting an increased MLCT contribution for a structureless profile. In addition, the radiative rate constant ( $k_r$ ) for Cb1 to Cb3 ( $2.0$ ,  $3.2$  and  $3.4 \times 10^5 \text{ s}^{-1}$ ), which was calculated from quantum yield ( $\Phi$ ) divided by the observed lifetime ( $\tau_{\text{obs}}$ ), revealed an ascending trend to the increased MLCT contribution, as it fostered stronger spin-orbital coupling and faster phosphorescence. This tendency was also observed by comparing the second set of the Ir(III) complexes Cb4 and Cb5, with the radiative rate constant being  $2.9 \times 10^5 \text{ s}^{-1}$  and  $3.3 \times 10^5 \text{ s}^{-1}$ , respectively. Furthermore, for Cb3 and Cb5, the bathochromic shift can also be rationalized with the electron-donating effect of NMe<sub>2</sub> substituent at the 4-position of pyridinyl group, giving a higher-lying HOMO level and hence a narrower energy gap.

Figure 3 shows the electrochemical properties of bis-tridentate Ir(III) complexes Cb1–5, with numerical data listed in Table 2. All complexes present reversible oxidation and irreversible reduction waves. Replacing CF<sub>3</sub> with the *tert*-butyl substituent in the monoanionic carbene pincer chelate induces a cathodic shift on the oxidation potential, e.g., Cb1 (0.56 V) to Cb4 (0.35 V). For Cb1, Cb2 and Cb3, the oxidation potentials experience a decrease from 0.56 V and 0.53 V to 0.45 V, with changing 4-hydrogen atom on the pyridinyl fragment to methoxy and dimethylamino substituents. A similar trend is also observed between Cb4 and Cb5, which varied from 0.35 V to 0.25 V, after the introduction of the

dimethylamino group. Meanwhile, the reduction potentials are also influenced by the substituent effect as mentioned earlier. Among Ir(III) complexes **Cb1–3**, **Cb3** exhibits the most destabilized LUMO by giving the most negative potential at  $-2.48$  V, which can be explained by the strongest electron-donating ability of the dimethylamino group. Moreover, both the Ir(III) complexes **Cb4** and **Cb5** ( $-2.50$  V and  $-2.56$  V, respectively) with the *tert*-butyl substituent on the monoanionic tridentate chelate display more negative reduction potentials than that of the  $\text{CF}_3$  substituted counterparts **Cb1**, **Cb2** and **Cb3** ( $-2.42$  V,  $-2.45$  V and  $-2.48$  V, respectively), showing that the LUMO is not associated with this pyridinyl coordination unit.

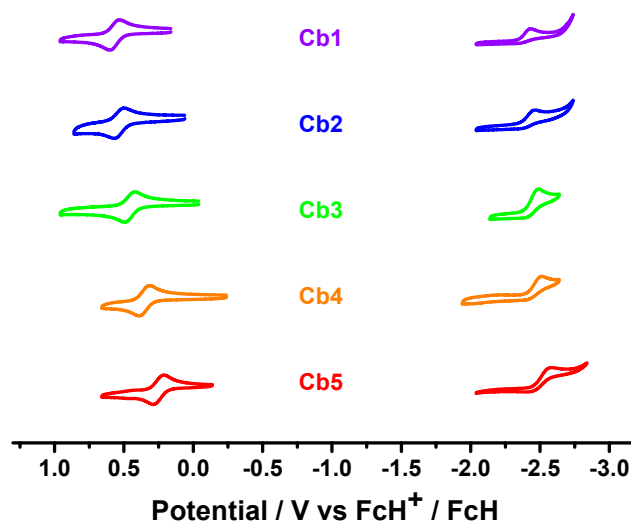


Figure 3. Cyclic voltammograms of Ir(III) metal complexes **Cb1–5**.

Table 2. Electrochemical data of the Ir(III) metal complexes **Cb1–5** in acetonitrile at RT.

	$E^{\text{ox}}_{1/2}$ (V) ( $\Delta E_p$ ) <sup>[a]</sup>	$E^{\text{re}}_{\text{pc}}$ (V) <sup>[b]</sup>	HOMO (eV) <sup>[c]</sup>	Energy Gap (eV) <sup>[d]</sup>	LUMO (eV) <sup>[e]</sup>
<b>Cb1</b>	0.56 (0.07)	$-2.42$	$-5.36$	2.64	$-2.72$
<b>Cb2</b>	0.53 (0.07)	$-2.45$	$-5.33$	2.66	$-2.67$
<b>Cb3</b>	0.45 (0.07)	$-2.48$	$-5.25$	2.65	$-2.60$
<b>Cb4</b>	0.35 (0.08)	$-2.50$	$-5.15$	2.52	$-2.63$
<b>Cb5</b>	0.25 (0.07)	$-2.56$	$-5.05$	2.53	$-2.52$

<sup>[a]</sup> All electrochemical potentials were measured in a 0.1 M acetonitrile solution of TBAPF<sub>6</sub> and reported in volts using Fc<sup>+</sup>/Fc as the reference.  $E^{\text{ox}}_{1/2}$  (V) refers to  $[(E_{\text{pa}} + E_{\text{pc}})/2]$ , where  $E_{\text{pa}}$  and  $E_{\text{pc}}$  are anodic and cathodic waves, respectively.  $\Delta E_p = E_{\text{pa}} - E_{\text{pc}}$ ; <sup>[b]</sup>  $E^{\text{re}}_{\text{pc}}$  is the cathodic wave potential for the irreversible reduction wave; <sup>[c]</sup> HOMO =  $-(E^{\text{ox}}_{1/2} + 4.8)$ ; <sup>[d]</sup> energy gap =  $1240/[\text{PL onset (nm)}]$ ; <sup>[e]</sup> LUMO = HOMO + Energy gap.

### 3.3. Theoretical Calculation

We then conducted the density functional theory (DFT) calculations at PBE0/LANL2DZ (Ir) and PBE0/6-31g(d,p) (H, C, N, F, O) levels using CH<sub>2</sub>Cl<sub>2</sub> as the solvent to optimize the ground-state ( $S_0$ ) geometries of all molecules. In addition, time-dependent (TD) DFT calculations at the same levels were performed to optimize the geometries of the excited states and to probe the transition characteristics of the studied Ir(III) complexes. The calculated transition energies and major assignments of Ir(III) complexes **Cb1–5** in CH<sub>2</sub>Cl<sub>2</sub> solution are summarized in Tables 3 and S1–S5, respectively. The frontier molecular orbitals involved in the major transitions were also depicted in Figures 4 and S1–S5. The calculated  $S_0 \rightarrow S_1$  transition in terms of wavelength was estimated to be **Cb1**: 402.7 nm, **Cb2**: 391.2 nm, **Cb3**: 394.8 nm, **Cb4**: 417.8 nm and **Cb5**: 413.4 nm, which are close to the onset of the absorption spectra in Figure 2. After structural optimization of the excited states  $S_1$  and  $T_1$ , the computed wavelengths for  $S_1 \rightarrow S_0$  and  $T_1 \rightarrow S_0$  vertical transition were **Cb1**: 488.2 and 588.4 nm, **Cb2**: 484.2 and 573 nm, **Cb3**: 490 and 557.4 nm, **Cb4**: 511

and 587.7 nm and **Cb5**: 520.2 and 598.9 nm, respectively. For **Cb1–5**, the calculated  $S_1 \rightarrow S_0$  wavelengths were all close to the onset of the emission spectra while the  $T_1 \rightarrow S_0$  wavelengths were akin to the experimental emissive peaks as recorded in Figure 2. The trends of  $S_0 \rightarrow S_1$  absorption and  $T_1 \rightarrow S_0$  emission were in good agreement with their corresponding absorption and phosphorescence spectra, respectively.

**Table 3.** The main transition characters, calculated wavelengths and contributing percentages of the lowest energy absorption and emission bands of Ir(III) complexes **Cb1–5** in  $\text{CH}_2\text{Cl}_2$  solution.

Complex	State	$\lambda$ (nm)	$f$	Main Assignments	MLCT
<b>Cb1</b>	$S_0 \rightarrow T_1$	459.1	0	HOMO $\rightarrow$ LUMO + 1 (19%)	13.52%
	$S_0 \rightarrow S_1$	402.7	0.0105	HOMO $\rightarrow$ LUMO + 1 (87%)	24.82%
	$T_1 \rightarrow S_0$	588.4	0	LUMO $\rightarrow$ HOMO (72%)	18.97%
	$S_1 \rightarrow S_0$	488.2	0.0083	LUMO $\rightarrow$ HOMO (96%)	30.30%
<b>Cb2</b>	$S_0 \rightarrow T_1$	449.2	0	HOMO $\rightarrow$ LUMO (29%)	18.62%
	$S_0 \rightarrow S_1$	391.2	0.0425	HOMO $\rightarrow$ LUMO (94%)	29.18%
	$T_1 \rightarrow S_0$	573	0	LUMO $\rightarrow$ HOMO (73%)	20.40%
	$S_1 \rightarrow S_0$	484.2	0.053	LUMO $\rightarrow$ HOMO (98%)	30.01%
<b>Cb3</b>	$S_0 \rightarrow T_1$	437.4	0	HOMO $\rightarrow$ LUMO (26%)	19.13%
	$S_0 \rightarrow S_1$	394.8	0.0509	HOMO $\rightarrow$ LUMO (94%)	30.36%
	$T_1 \rightarrow S_0$	557.4	0	LUMO $\rightarrow$ HOMO (72%)	19.92%
	$S_1 \rightarrow S_0$	490	0.0553	LUMO $\rightarrow$ HOMO (98%)	31.27%
<b>Cb4</b>	$S_0 \rightarrow T_1$	462.1	0	HOMO $\rightarrow$ LUMO + 1 (87%)	23.64%
	$S_0 \rightarrow S_1$	417.8	0.0074	HOMO $\rightarrow$ LUMO + 1 (85%)	23.09%
	$T_1 \rightarrow S_0$	587.7	0	LUMO $\rightarrow$ HOMO (72%)	19.15%
	$S_1 \rightarrow S_0$	511	0.0062	LUMO $\rightarrow$ HOMO (96%)	27.39%
<b>Cb5</b>	$S_0 \rightarrow T_1$	449.5	0	HOMO $\rightarrow$ LUMO (83%)	25.75%
	$S_0 \rightarrow S_1$	413.4	0.0432	HOMO $\rightarrow$ LUMO (96%)	29.78%
	$T_1 \rightarrow S_0$	598.9	0	LUMO $\rightarrow$ HOMO (76%)	23.85%
	$S_1 \rightarrow S_0$	520.2	0.0423	LUMO $\rightarrow$ HOMO (98%)	28.86%

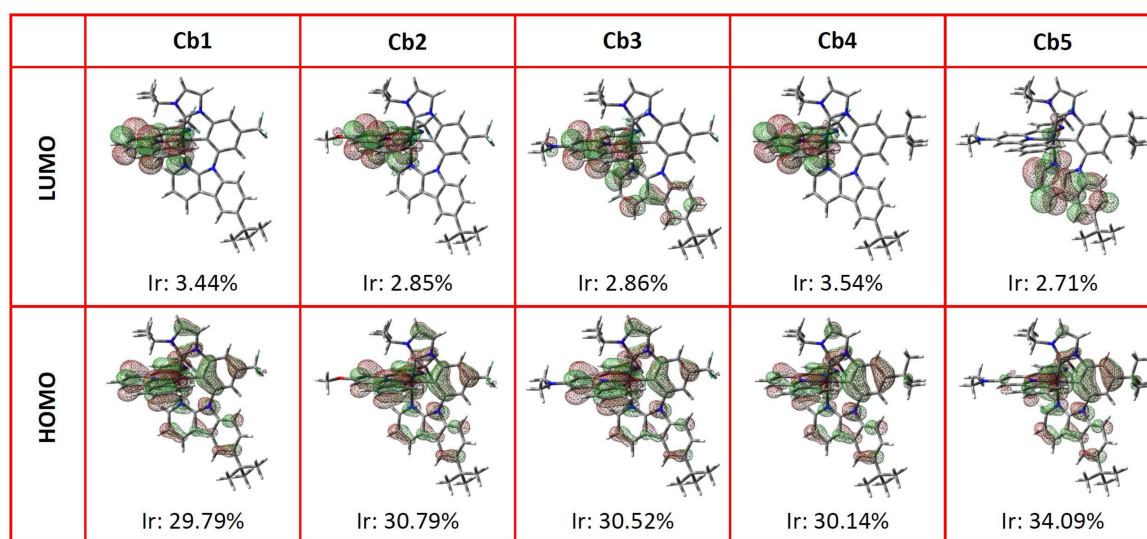


**Figure 4.** Frontier molecular orbitals HOMO and LUMO in the  $T_1$  excited state for the Ir(III) complexes **Cb1–5** in  $\text{CH}_2\text{Cl}_2$  solution. “Ir” indicates the relative electron density distribution at the Ir atoms.

Moreover, the  $S_0 \rightarrow S_1$  absorption was derived mainly from HOMO  $\rightarrow$  LUMO+1 for **Cb1** and **Cb4** and HOMO  $\rightarrow$  LUMO for **Cb2**, **Cb3** and **Cb5**, respectively (Table 3). The  $S_1 \rightarrow S_0$  and  $T_1 \rightarrow S_0$  emission were all assigned to LUMO  $\rightarrow$  HOMO for **Cb1–5**. For the ground state  $S_0$  of **Cb1–5**, the electron density distribution of the HOMO was mainly localized at the central Ir(III) metal atom (31–34%) and delocalized over the chromophoric chelate 2-phenyl-6-(3-(trifluoromethyl)-1H-pyrazol-5-yl)pyridine (phyz) and carbene-benzene-carboline (cb), while the electron density distribution of the LUMO and LUMO+1 was mainly localized at the cb or phyz chelate, respectively, accompanying a little contribution at the Ir(III) atom (1–3%) (Figures 4 and S1–S5). For the excited states  $S_1$  and  $T_1$  of **Cb1–5**, the electron density distribution of the HOMO was mainly localized

at the central Ir(III) metal atom (29–36%) and delocalized over the phyz and cb fragment, while the electron density distribution of the LUMO was mainly localized at the cb or phyz chelate, together with a few contribution at the Ir(III) atom (2–4%). Moreover, it is notable that LUMO is partially shifted to carboline moiety in **Cb3**, while completely moved to carboline moiety as observed in **Cb5**. We attributed this to the introducing of the dimethylamino substituent at the pyridinyl unit of the dianionic chelate that greatly increased the associated  $\pi^*$  orbital energy, such that the LUMO is now dominated by the relatively unaffected carboline  $\pi^*$  orbital. Overall, the  $S_0 \rightarrow S_1$ ,  $S_1 \rightarrow S_0$  and  $T_1 \rightarrow S_0$  transitions were all mainly ascribed to the metal-to-ligand charge transfer (MLCT) process (19–31%), accompanied by minor ligand-to-ligand charge transfer (LLCT) or intraligand charge transfer (ILCT). These high MLCT characters were in nice relevance to the moderate emission quantum yield (41–69%) of the emissive complexes **Cb1–5** in Tables 1 and 3. Furthermore, with regard to the calculated HOMO energy levels of  $S_0$ ,  $S_1$  and  $T_1$ , **Cb3** was higher than **Cb1** and **Cb2** due to the electron-donating effect of NMe<sub>2</sub> substituent at the 4-position of pyridinyl group in **Cb3**. Additionally, **Cb5** is higher than that of **Cb4** (Table 2 and Figures S1–S5). The trend of calculated HOMO energy levels is in good agreement with the experimental results (vide supra).

### 3.4. Fabrication of OLED Devices

All these new Ir(III) complexes showed a high decomposition temperature (>283 °C, Figure S6), which is suitable for conducting device fabrication via thermal deposition. In view of their better photophysical properties, **Cb1** and **Cb4** were selected as the dopant emitter in fabrication of OLED devices with architecture: ITO/TAPC (40 nm)/TCTA (10 nm)/mCP (10 nm)/8 wt.% dopant in mCP (20 nm)/TmPyPB (45 nm)/LiF (1 nm)/Al. Figure 5 presents the chemical structures of the employed materials and device configuration. The obtained device characteristics and key parameters are summarized in Figure 6 and Table 4 for scrutiny. Here, 1,1-bis((di-4-tolylamino)phenyl)cyclohexane (TAPC) and tris(4-carbazoyl-9-ylphenyl)amine (TCTA) are taken as the hole-transporting and electron-blocking layer. 1,3-Bis(N-carbazoyl)benzene (mCP) serves as both the hole-blocking layer and host in the emissive layer. 1,3,5-Tri(3-pyridyl-3-phenyl)benzene (TmPyPB), LiF and Al are acting as the electron-transporting layer, electron injection layer and cathode, respectively.

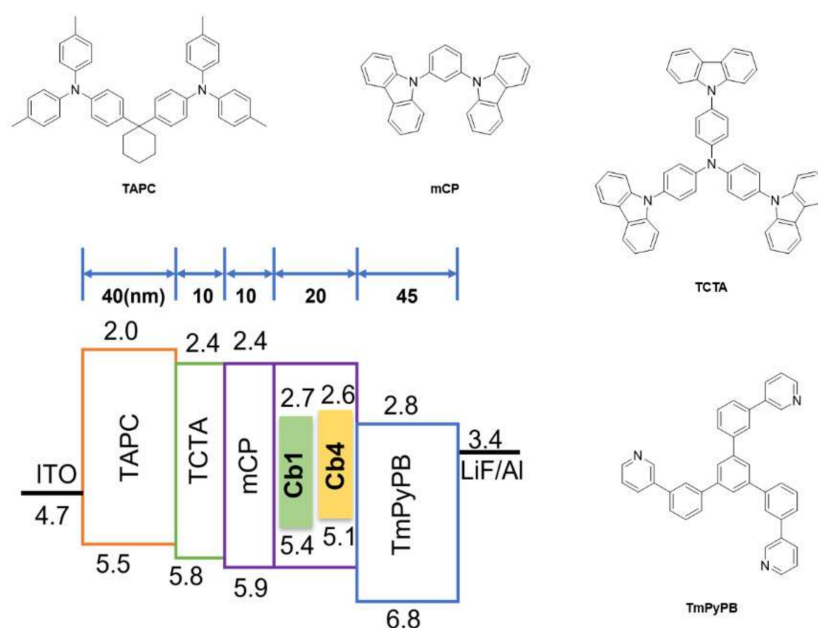


**Figure 5.** Schematic device configuration, energy level diagram and chemical structures of the materials used in devices.

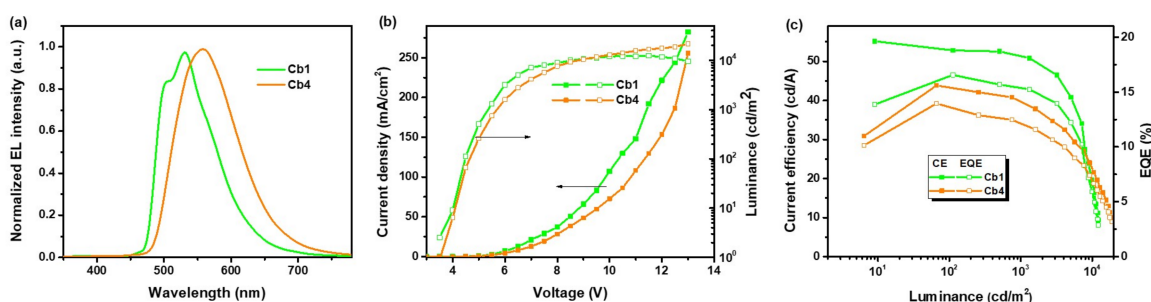


**Figure 6.** Summary of electroluminescence data: (a) normalized EL spectra of **Cb1** and **Cb4**, (b) current density-voltage-luminance (J-V-L) characteristics and (c) plot of current efficiency-luminance-EQE.

**Table 4.** Device performances of OLEDs based on bis-tridentate Ir(III) complexes **Cb1** and **Cb4**.

	$\lambda_{EL}$ [nm]	$V_{on}$ [V] [a]	Max. Luminescence [cd/m <sup>2</sup> ] (@voltage [V])	EQE [%] [b]	CE [cd/A] [b]
<b>Cb1</b>	503(sh), 530	3.5	12420 (11.5)	16.6, 16.5, 15.4	55.2, 52.9, 51.1
<b>Cb4</b>	559	3.5	21480 (13)	13.9, 13.1, 12.1	43.8, 43.0, 38.8

[a] Voltage at 1 cd/m<sup>2</sup>; [b] data recorded at maximum efficiency, 100 and 1000 cd/m<sup>2</sup>, respectively.

As showed in Figure 6, their normalized EL spectra resemble the PL spectra recorded in the degassed CH<sub>2</sub>Cl<sub>2</sub> solution, confirming that the emission is solely generated from the emitters, from which EL of **Cb4** is also red-shifted compared to that of **Cb1**. Moreover, the **Cb4**-based device shows a relatively lower current density at the same voltage compared to that of the **Cb1**-based device, which can be ascribed to the carrier trapping effect of **Cb4** with a narrower energy gap than that of **Cb1** [45,46]. In contrast, the **Cb1**-based device exhibited a bright green emission with EL peak at 530 nm and a maximum luminance of 12,420 cd/m<sup>2</sup> at 11.5 V, while the **Cb4**-based device delivered a yellow EL peak centered at 559 nm with a maximum luminance of 21,480 cd/m<sup>2</sup> at 13.0 V. A maximum external quantum efficiency (current efficiency) of 16.6% (55.2 cd/A) and 13.9% (43.8 cd/A) was also observed for **Cb1**- and **Cb4**-based devices, respectively. More importantly, both OLED devices present a small efficiency roll-off at 1000 cd/m<sup>2</sup> (15.4% and 12.1% for **Cb1** and **Cb4**-based devices, respectively), evidencing good carrier balance during device operation.

#### 4. Conclusions

In summary, by introducing varied substituents at the 4-position of central pyridinyl fragment of dianionic chelate or on the central phenyl coordination unit of carboline-based monoanionic pincer chelate, a series of five bis-tridentate Ir(III) complexes were successfully designed and synthesized, with an isolation yield higher than 50% and absence of any isomeric product. This result is consistent with those documented in literature [37,43]. The addition of methoxy and dimethylamino substituents at the 4-position of central pyridinyl fragment of dianionic chelate effectively increased the electron density at the Ir(III) metal center, which increased the MLCT contribution at the excited states, and gave a structureless emission profile. As for Ir(III) complexes **Cb4** and **Cb5**, the *tert*-butyl substituent on the 4-position of the phenyl ring also red-shifted the emission and exhibited slightly reduced emission quantum yields. Next, **Cb1** and **Cb4** were doped into the emission layer for fabrication of OLEDs, achieving a maximum external quantum efficiency (current efficiency) of 16.6% (55.2 cd/A) and 13.9% (43.8 cd/A), respectively. The well-performed electroluminescence efficiencies indicate that the studied bis-tridentate Ir(III) complexes and their future derivations are promising candidates for OLED applications.

**Supplementary Materials:** The following are available online. General experimental procedures of all measurements and calculations, synthetic protocol of chelates, original electrochemical data and detailed TD-DFT results of studied Ir(III) metal complexes. Scheme S1. Synthetic protocol given the employed dianionic chelates (phyz)H<sub>2</sub>; Scheme S2. Synthetic protocol given the employed carboline

chelates (cbF)H·HF<sub>6</sub> and (cbB)H·HF<sub>6</sub>; Figure S1. Frontier molecular orbitals pertinent to the optical transitions for the ground state S<sub>0</sub>, excited state T<sub>1</sub> and S<sub>1</sub> of Ir(III) complex **Cb1**. The electron density distributions of Ir atoms in each molecular orbital are shown; Figure S2. Frontier molecular orbitals pertinent to the optical transitions for the ground state S<sub>0</sub>, excited state T<sub>1</sub> and S<sub>1</sub> of Ir(III) complex **Cb2**. The electron density distributions of Ir atoms in each molecular orbital are shown; Figure S3. Frontier molecular orbitals pertinent to the optical transitions for the ground state S<sub>0</sub>, excited state T<sub>1</sub> and S<sub>1</sub> of Ir(III) complex **Cb3**. The electron density distributions of Ir atoms in each molecular orbital are shown; Figure S4. Frontier molecular orbitals pertinent to the optical transitions for the ground state S<sub>0</sub>, excited state T<sub>1</sub> and S<sub>1</sub> of Ir(III) complex **Cb4**. The electron density distributions of Ir atoms in each molecular orbital are shown; Figure S5. Frontier molecular orbitals pertinent to the optical transitions for the ground state S<sub>0</sub>, excited state T<sub>1</sub> and S<sub>1</sub> of Ir(III) complex **Cb5**. The electron density distributions of Ir atoms in each molecular orbital are shown; Figure S6. Thermal gravimetric analysis of studied Ir(III) complexes **Cb 1–5** with a decomposition temperature (T<sub>d</sub>) showing a loss of 5% in weight; Table S1. The calculated wavelengths, transition probabilities and charge transfer character of the optical transitions for Ir(III) complex **Cb1** in CH<sub>2</sub>Cl<sub>2</sub>; Table S2. The calculated wavelengths, transition probabilities and charge transfer character of the optical transitions for Ir(III) complex **Cb2** in CH<sub>2</sub>Cl<sub>2</sub>; Table S3. The calculated wavelengths, transition probabilities and charge transfer character of the optical transitions for Ir(III) complex **Cb3** in CH<sub>2</sub>Cl<sub>2</sub>; Table S4. The calculated wavelengths, transition probabilities and charge transfer character of the optical transitions for Ir(III) complex **Cb4** in CH<sub>2</sub>Cl<sub>2</sub>; Table S5. The calculated wavelengths, transition probabilities and charge transfer character of the optical transitions for Ir(III) complex **Cb5** in CH<sub>2</sub>Cl<sub>2</sub>.

**Author Contributions:** Conceptualization, J.Y. and Y.C.; methodology, J.Y., Z.-L.Z., S.-H.L., P.-T.C. and Y.C.; software, J.Y., Z.-L.Z., S.-H.L., P.-T.C. and Y.C.; validation, C.-S.L., P.-T.C. and Y.C.; writing—original draft preparation, J.Y., S.-H.L. and Y.C.; writing—review and editing, Z.-L.Z., P.-T.C. and Y.C. All authors have read and agreed to the published version of the manuscript.

**Funding:** This research was mainly funded by NSFC–NSFC/RGC Joint Research Scheme, grant number N\_CityU102/19.

**Institutional Review Board Statement:** Not applicable.

**Informed Consent Statement:** Not applicable.

**Data Availability Statement:** The data presented in this study are available in the Supplementary Materials.

**Acknowledgments:** This work was also partially supported by fundings from Research Grant Council and City University of Hong Kong, Hong Kong SAR. Works conducted in Taiwan were supported by Ministry of Science and Technology (MOST) and National Taiwan University. We were also grateful to the National Center for High-Performance Computing (NCHC) of Taiwan for the valuable computer time and research facilities.

**Conflicts of Interest:** The authors declare no conflict of interest.

## References

1. Liu, D.-S.; Wu, J.; Xu, H.; Wang, Z. Emerging Light-Emitting Materials for Photonic Integration. *Adv. Mater.* **2021**, *33*, 2003733. [[CrossRef](#)] [[PubMed](#)]
2. Chou, P.-T.; Chi, Y. Phosphorescent dyes for organic light-emitting diodes. *Chem. Eur. J.* **2007**, *13*, 380–395. [[CrossRef](#)] [[PubMed](#)]
3. Chi, Y.; Chou, P.-T. Transition Metal Phosphors with Cyclometalating Ligands; Fundamental and Applications. *Chem. Soc. Rev.* **2010**, *39*, 638–655. [[CrossRef](#)]
4. Henwood, A.F.; Zysman-Colman, E. Lessons Learned in Tuning the Optoelectronic Properties of Phosphorescent Iridium(III) Complexes. *Chem. Commun.* **2017**, *53*, 807–826. [[CrossRef](#)]
5. Li, T.-Y.; Wu, J.; Wu, Z.-G.; Zheng, Y.-X.; Zuo, J.-L.; Pan, Y. Rational Design of Phosphorescent Iridium(III) Complexes for Emission Color Tunability and Their Applications in OLEDs. *Coord. Chem. Rev.* **2018**, *374*, 55–92. [[CrossRef](#)]
6. Li, G.; Congrave, D.G.; Zhu, D.; Su, Z.; Bryce, M.R. Recent advances in luminescent dinuclear iridium(III) complexes and their application in organic electroluminescent devices. *Polyhedron* **2018**, *140*, 146–157. [[CrossRef](#)]
7. Li, G.; Zhu, D.; Wang, X.; Su, Z.; Bryce, M.R. Dinuclear metal complexes: Multifunctional properties and applications. *Chem. Soc. Rev.* **2020**, *49*, 765–838. [[CrossRef](#)]
8. Sajoto, T.; Djurovich, P.I.; Tamayo, A.; Yousufuddin, M.; Bau, R.; Thompson, M.E.; Holmes, R.J.; Forrest, S.R. Blue and Near-UV Phosphorescence from Iridium Complexes with Cyclometalated Pyrazolyl or N-Heterocyclic Carbene Ligands. *Inorg. Chem.* **2005**, *44*, 7992–8003. [[CrossRef](#)] [[PubMed](#)]

9. Daniels, R.E.; Culham, S.; Hunter, M.; Durrant, M.C.; Probert, M.R.; Clegg, W.; Williams, J.A.G.; Kozhevnikov, V.N. When two are better than one: Bright phosphorescence from non-stereogenic dinuclear iridium(III) complexes. *Dalton Trans.* **2016**, *45*, 6949–6962. [[CrossRef](#)]
10. Yan, Z.-P.; Luo, X.-F.; Liao, K.; Lin, Z.-X.; Wu, Z.-G.; Zhou, Y.-H.; Zheng, Y.-X. The Taiji and Eight Trigrams chemistry philosophy of chiral iridium(III) complexes with triplex stereogenic centers. *Dalton Trans.* **2018**, *47*, 4045–4048. [[CrossRef](#)]
11. Shafikov, M.Z.; Martinscroft, R.; Hodgson, C.; Hayer, A.; Auch, A.; Kozhevnikov, V.N. Non-Stereogenic Dinuclear Ir(III) Complex with a Molecular Rack Design to Afford Efficient Thermally Enhanced Red Emission. *Inorg. Chem.* **2021**, *60*, 1780–1789. [[CrossRef](#)]
12. Chi, Y.; Chang, T.-K.; Ganesan, P.; Rajakannu, P. Emissive Bis-Tridentate Ir(III) Metal Complexes: Tactics, Photophysics and Applications. *Coord. Chem. Rev.* **2017**, *346*, 91–100. [[CrossRef](#)]
13. Pandit, V.; Jang, J.; Babazadeh, M.; Ranasinghe, C.S.K.; Huang, D.M.; Burn, P.L.; Puttock, E.V. A solution-processed bis-tridentate iridium(III) complex-cored dendrimer for green OLEDs. *J. Mater. Chem. C* **2021**. [[CrossRef](#)]
14. Williams, J.A.G. The coordination chemistry of dipyritylbenzene: N-deficient terpyridine or panacea for brightly luminescent metal complexes? *Chem. Soc. Rev.* **2009**, *38*, 1783–1801. [[CrossRef](#)]
15. Pal, A.K.; Hanan, G.S. Design, synthesis and excited-state properties of mononuclear Ru(II) complexes of tridentate heterocyclic ligands. *Chem. Soc. Rev.* **2014**, *43*, 6184–6197. [[CrossRef](#)] [[PubMed](#)]
16. Braun, J.D.; Lozada, I.B.; Kolodziej, C.; Burda, C.; Newman, K.M.E.; van Lierop, J.; Davis, R.L.; Herbert, D.E. Iron(II) coordination complexes with panchromatic absorption and nanosecond charge-transfer excited state lifetimes. *Nat. Chem.* **2019**, *11*, 1144–1150. [[CrossRef](#)] [[PubMed](#)]
17. Wilkinson, A.J.; Goeta, A.E.; Foster, C.E.; Williams, J.A.G. Synthesis and Luminescence of a Charge-Neutral, Cyclometalated Iridium(III) Complex Containing N<sup>+</sup>C<sup>-</sup>N<sup>-</sup> and C<sup>-</sup>N<sup>+</sup>C<sup>-</sup>-Coordinating Tridentate Ligands. *Inorg. Chem.* **2004**, *43*, 6513–6515. [[CrossRef](#)]
18. Koga, Y.; Kamo, M.; Yamada, Y.; Matsumoto, T.; Matsubara, K. Synthesis, Structures, and Unique Luminescent Properties of Tridentate C<sup>-</sup>C<sup>-</sup>N Cyclometalated Complexes of Iridium. *Eur. J. Inorg. Chem.* **2011**, *2011*, 2869–2878. [[CrossRef](#)]
19. Esteruelas, M.A.; Gómez-Bautista, D.; López, A.M.; Oñate, E.; Tsai, J.-Y.; Xia, C.  $\eta^1$ -Arene Complexes as Intermediates in the Preparation of Molecular Phosphorescent Iridium(III) Complexes. *Chem. Eur. J.* **2017**, *23*, 15729–15737. [[CrossRef](#)]
20. Boudreault, P.-L.T.; Esteruelas, M.A.; Gómez-Bautista, D.; Izquierdo, S.; López, A.M.; Oñate, E.; Raga, E.; Tsai, J.-Y. Preparation and Photophysical Properties of Bis(tridentate) Iridium(III) Emitters: Pincer Coordination of 2,6-Di(2-pyridyl)phenyl. *Inorg. Chem.* **2020**, *59*, 3838–3849. [[CrossRef](#)] [[PubMed](#)]
21. Kuei, C.-Y.; Liu, S.-H.; Chou, P.-T.; Lee, G.-H.; Chi, Y. Room Temperature Blue Phosphorescence; A Combined Experimental and Theoretical Study on the Bis-tridentate Ir(III) Metal Complexes. *Dalton Trans.* **2016**, *45*, 15364–15373. [[CrossRef](#)]
22. Kuei, C.-Y.; Tsai, W.-L.; Tong, B.; Jiao, M.; Lee, W.-K.; Chi, Y.; Wu, C.-C.; Liu, S.-H.; Lee, G.-H.; Chou, P.-T. Bis-Tridentate Ir(III) Complexes with Nearly Unitary RGB Phosphorescence and Organic Light-Emitting Diodes with External Quantum Efficiency Exceeding 31%. *Adv. Mater.* **2016**, *28*, 2795–2800. [[CrossRef](#)]
23. Kuo, H.-H.; Chen, Y.-T.; Devereux, L.R.; Wu, C.-C.; Fox, M.A.; Kuei, C.-Y.; Chi, Y.; Lee, G.-H. Bis-Tridentate Ir(III) Metal Phosphors for Efficient Deep-Blue Organic Light-Emitting Diodes. *Adv. Mater.* **2017**, *29*, 1702464. [[CrossRef](#)]
24. Kuo, H.-H.; Zhu, Z.-L.; Lee, C.-S.; Chen, Y.-K.; Liu, S.-H.; Chou, P.-T.; Jen, A.K.-Y.; Chi, Y. Bis-tridentate Iridium(III) Phosphors with Very High Photostability and Fabrication of Blue-Emitting OLEDs. *Adv. Sci.* **2018**, *5*, 1800846. [[CrossRef](#)] [[PubMed](#)]
25. Tong, B.; Ku, H.Y.; Chen, I.J.; Chi, Y.; Kao, H.-C.; Yeh, C.-C.; Chang, C.-H.; Liu, S.-H.; Lee, G.-H.; Chou, P.-T. Heteroleptic Ir(III) Phosphors with Bis-Tridentate Chelating Architecture for High Efficiency OLEDs. *J. Mater. Chem. C* **2015**, *3*, 3460–3471. [[CrossRef](#)]
26. Lin, J.; Chau, N.-Y.; Liao, J.-L.; Wong, W.-Y.; Lu, C.-Y.; Sie, Z.-T.; Chang, C.-H.; Fox, M.A.; Low, P.J.; Lee, G.-H.; et al. Bis-Tridentate Iridium(III) Phosphors Bearing Functional 2-Phenyl-6-(imidazol-2-ylidene)pyridine and 2-(Pyrazol-3-yl)-6-phenylpyridine Chelates for Efficient OLEDs. *Organometallics* **2016**, *35*, 1813–1824. [[CrossRef](#)]
27. Lin, J.; Wang, Y.; Gnanasekaran, P.; Chiang, Y.-C.; Yang, C.-C.; Chang, C.-H.; Liu, S.-H.; Lee, G.-H.; Chou, P.-T.; Chi, Y.; et al. Unprecedented Homoleptic Bis-Tridentate Iridium(III) Phosphors: Facile, Scaled-Up Production, and Superior Chemical Stability. *Adv. Funct. Mater.* **2017**, *27*, 1702856. [[CrossRef](#)]
28. Hsu, L.-Y.; Chen, D.-G.; Liu, S.-H.; Chiu, T.-Y.; Chang, C.-H.; Jen, A.K.Y.; Chou, P.-T.; Chi, Y. Roles of Ancillary Chelates and Overall Charges of Bis-tridentate Ir(III) Phosphors for OLED Applications. *ACS Appl. Mater. Interfaces* **2020**, *12*, 1084–1093. [[CrossRef](#)]
29. Zheng, Y.; Batsanov, A.S.; Edkins, R.M.; Beeby, A.; Bryce, M.R. Thermally Induced Defluorination during a mer to fac Transformation of a Blue-Green Phosphorescent Cyclometalated Iridium(III) Complex. *Inorg. Chem.* **2012**, *51*, 290–297. [[CrossRef](#)]
30. Zhang, D.-Y.; Zheng, Y.; Zhang, H.; Sun, J.-H.; Tan, C.-P.; He, L.; Zhang, W.; Ji, L.-N.; Mao, Z.-W. Delivery of Phosphorescent Anticancer Iridium(III) Complexes by Polydopamine Nanoparticles for Targeted Combined Photothermal-Chemotherapy and Thermal/Photoacoustic/Lifetime Imaging. *Adv. Sci.* **2018**, *5*, 1800581. [[CrossRef](#)]
31. Motoyama, T.; Sasabe, H.; Seino, Y.; Takamatsu, J.-i.; Kido, J. An  $\alpha$ -Carboline-containing Host Material for High-efficiency Blue and Green Phosphorescent OLEDs. *Chem. Lett.* **2011**, *40*, 306–308. [[CrossRef](#)]
32. Cho, M.J.; Kim, S.J.; Yoon, S.H.; Shin, J.; Hong, T.R.; Kim, H.J.; Son, Y.H.; Kang, J.S.; Um, H.A.; Lee, T.W.; et al. New Bipolar Host Materials for Realizing Blue Phosphorescent Organic Light-Emitting Diodes with High Efficiency at 1000 cd/m<sup>2</sup>. *ACS Appl. Mater. Interfaces* **2014**, *6*, 19808–19815. [[CrossRef](#)] [[PubMed](#)]

33. Wang, Y.-K.; Deng, Y.-L.; Liu, X.-Y.; Yuan, X.-D.; Jiang, Z.-Q.; Liao, L.-S. A facile way to synthesize high-triplet-energy hosts for blue phosphorescent organic light-emitting diodes with high glass transition temperature and low driving voltage. *Dyes and Pigment.* **2015**, *122*, 6–12. [[CrossRef](#)]
34. Wu, Q.; Wang, M.; Cao, X.; Zhang, D.; Sun, N.; Wan, S.; Tao, Y. Carbazole/ $\alpha$ -carboline hybrid bipolar compounds as electron acceptors in exciplex or non-exciplex mixed cohosts and exciplex-TADF emitters for high-efficiency OLEDs. *J. Mater. Chem. C* **2018**, *6*, 8784–8792. [[CrossRef](#)]
35. Wang, H.; Zhao, H.; Zang, C.; Liu, S.; Zhang, L.; Xie, W. Stable and efficient phosphorescent organic light-emitting device utilizing a  $\delta$ -carboline-containing host displaying thermally activated delayed fluorescence. *J. Mater. Chem. C* **2020**, *8*, 3800–3806. [[CrossRef](#)]
36. Neumann, U.; Vögtle, F. 4,4'-Donor-substituierte und 6,6'-difunktionalisierte 2,2'-Bipyridine. *Chem. Ber.* **1989**, *122*, 589–591. [[CrossRef](#)]
37. Zhu, Z.-L.; Chen, W.-C.; Ni, S.-F.; Yan, J.; Wang, S.F.; Fu, L.-W.; Tsai, H.-Y.; Chi, Y.; Lee, C.-S. Constructing Deep-Blue Bis-tridentate Ir(III) Phosphors with Fluorene-Based Dianionic Chelates. *J. Mater. Chem. C* **2021**, *9*, 1318–1325. [[CrossRef](#)]
38. Mairhofer, E.; Flemmich, L.; Kreutz, C.; Micura, R. Access to 3-Deazaguanosine Building Blocks for RNA Solid-Phase Synthesis Involving Hartwig–Buchwald C–N Cross-Coupling. *Org. Lett.* **2019**, *21*, 3900–3903. [[CrossRef](#)]
39. Viricel, W.; Mbarek, A.; Leblond, J. Switchable Lipids: Conformational Change for Fast pH-Triggered Cytoplasmic Delivery. *Angew. Chem. Int. Ed.* **2015**, *54*, 12743–12747. [[CrossRef](#)]
40. He, L.; Allwein, S.P.; Dugan, B.J.; Knouse, K.W.; Ott, G.R.; Zifcick, C.A. Synthesis of  $\alpha$ -carboline. *Org. Synth.* **2016**, *93*, 272–293. [[CrossRef](#)]
41. Hsu, C.-W.; Ho, S.-T.; Wu, K.-L.; Chi, Y.; Liu, S.-H.; Chou, P.-T. Ru(II) sensitizers with a tridentate heterocyclic cyclometalate for dye-sensitized solar cells. *Energy Environ. Sci.* **2012**, *5*, 7549–7554. [[CrossRef](#)]
42. Tamayo, A.B.; Alleyne, B.D.; Djurovich, P.I.; Lamansky, S.; Tsyba, I.; Ho, N.N.; Bau, R.; Thompson, M.E. Synthesis and Characterization of Facial and Meridional Tris-cyclometalated Iridium(III) Complexes. *J. Am. Chem. Soc.* **2003**, *125*, 7377–7387. [[CrossRef](#)]
43. Tai, W.-S.; Gnanasekaran, P.; Chen, Y.-Y.; Hung, W.-Y.; Zhou, X.; Chou, T.-C.; Lee, G.-H.; Chou, P.-T.; You, C.; Chi, Y. Rational Tuning of Bis-Tridentate Ir(III) Phosphors to Deep-Blue with High Efficiency and Sub-microsecond Lifetime. *ACS Appl. Mater. Interfaces* **2021**, *13*, 15437–15447. [[CrossRef](#)] [[PubMed](#)]
44. Zhu, Z.L.; Hsu, L.Y.; Tai, W.S.; Ni, S.F.; Lee, C.S.; Chi, Y. Revealing the Role of 1,2,4-Triazole Fragment of Blue-Emitting Bis-tridentate Ir(III) Phosphors: Photophysical Properties, Photo-stabilities, and Applications. *Mater. Today Energy* **2021**, *20*, 100636. [[CrossRef](#)]
45. von Malm, N.; Steiger, J.; Schmechel, R.; von Seggern, H. Trap engineering in organic hole transport materials. *J. Appl. Phys.* **2001**, *89*, 5559–5563. [[CrossRef](#)]
46. Liao, J.-L.; Chi, Y.; Sie, Z.-T.; Ku, C.-H.; Chang, C.-H.; Fox, M.A.; Low, P.J.; Tseng, M.-R.; Lee, G.-H. Ir(III)-Based Phosphors with Bipyrazolate Ancillaries; Rational Design, Photophysics, and Applications in Organic Light-Emitting Diodes. *Inorg. Chem.* **2015**, *54*, 10811–10821. [[CrossRef](#)]